Kinetics of the Reaction of SH and SD with NO_2

Scott C. Herndon[†] and A. R. Ravishankara*

National Oceanic and Atmospheric Administration, Earth System Research Laboratory, Boulder, CO 80305, Department of Chemistry and Biochemistry, University of Colorado, Boulder, CO 80309, and The Cooperative Institute for Research in Environmental Sciences, University of Colorado, Boulder, CO 80309

Received: July 16, 2005; In Final Form: October 10, 2005

The rate constants for the reactions of NO_2 with SH and SD were measured between 250 and 360 K to be 2.8×10^{-11} exp{$(270 \pm 40)/T$(K)} and 2.6×10^{-11} exp{$(285 \pm 20)/T$(K)} cm^3 molecule^{-1} s^{-1}, respectively. SH(SD) radicals were generated by pulsed laser photolysis of $H_2S(D_2S)$ or CH_3SH and detected via pulsed laser-induced fluorescence. The laser-induced fluorescence excitation spectrum of SH was found to be contaminated by the presence of the SO radical. This contamination is suggested as a possible reason for differences among some of the reported values of k_1 in the literature. The title reaction influences the atmospheric lifetime of the SH radical when NO_2 is greater than 100 pptv, but the revised value of k_1 does not significantly alter our current understanding of SH oxidation in the atmosphere.

Introduction

Hydrogen sulfide (H_2S), emitted mostly by terrestrial sources, is an important natural reduced sulfur species in the troposphere. The tropospheric lifetime of H_2S is determined by its reaction with the OH radical (∼2.5 days), which leads to the formation of the SH radical.[1−3] Thermochemical considerations rule out H atom abstraction from aliphatic hydrocarbons by SH. The tropospheric loss of SH is governed by its reactions with O_3 and NO_2 and to a lesser extent NO. Accurate values of the rate coefficients are needed to assess the lifetime of the SH radical and to fully elucidate the mechanism for atmospheric oxidation of H_2S.

There are some differences between previously reported values of the rate coefficients for the reactions of SH with NO_2:

$$SH + NO_2 \rightarrow HSO + NO;\ k_{1a} \qquad (1a)$$

$$\xrightarrow{M} HSNO_2;\ k_{1b} \qquad (1b)$$

Reported values of k_1 ($k_1 = k_{1a} + k_{1b}$) range from 2.5×10^{-11} to 12×10^{-11} cm^3 molecule^{-1} s^{-1}. The range of literature values for k_1 could be due to the experimental difficulties involved in measuring this reaction rate coefficient. First, there is a dark reaction (likely on the walls) between NO_2 and H_2S, the commonly used precursor of SH. This potentially leads to uncertainties in the concentration of NO_2 in the reaction cell as well as production of species that enhance the loss or secondary production of SH. Second, SH reacts very rapidly with itself and other free radicals, such as OH and HO_2, requiring the use of low concentrations of SH in kinetics studies. Third, in photolysis systems, H atoms are unavoidably produced due to H_2S photodissociation. This could regenerate SH via the reaction $H + H_2S \rightarrow SH + H_2$ and lead to an apparent value of k_1 that is lower than the true value (see Results and Discussion for more details). Stachnik and Molina[4] used molecular oxygen to scavenge H atoms and obtained a lower value than that reported by Wang et al.[5] using a flow system. Stachnik and Molina took great care to minimize secondary reactions in their system. The lower value of Stachnik and Molina could be due to the suppression of secondary reactions or due to the complexing of SH with O_2 to form HSOO. If HSOO has a lower reactivity with NO_2 than SH, the loss of SH via reaction 1 would be offset by the dissociation of HSOO. The formation of HSOO has been suggested[6] on the basis of analogy with the reactivity of CH_3-SOO formed in the addition of CH_3S with O_2[7] and by ab initio calculations.[6]

In this work, the rate coefficient for reaction 1 was measured as a function of temperature. The rate coefficient for NO_2 reaction with SD, the deuterated analogue of SH, was also determined.

$$SD + NO_2 \rightarrow DSO + NO \qquad (2a)$$

$$\xrightarrow{M} DSNO_2 \qquad (2b)$$

The differences between k_1 and k_2 are expected to be very small because only a secondary kinetic isotope effect is anticipated. The rate coefficient for reaction 2, k_2, was measured as a further check on k_1.

During the course of our investigation of the SH detection via laser-induced fluorescence, we found the observed laser-induced fluorescence (LIF) spectrum near 323.7 nm, the $^RQ_{21}$ and R_1 band heads of SH, to be contaminated by a contribution by another species, which we believe is SO. These were the wavelengths used to monitor SH in some of the previous determinations of k_1. The possible impact of this spectral contamination on the measured value of k_1 was also investigated.

Experimental Description

The SH radicals were produced by pulsed 193 nm laser photolysis of H_2S or CH_3SH and were detected by laser-induced fluorescence. The temporal profiles of SH were measured in the presence of a large excess of NO_2, whose concentration in the reactor was determined using flow and/or absorption methods.

* Corresponding author. Present address: NOAA/ESRL R/CSD 2, 325 Broadway, Boulder, CO 80305. E-mail: a.r.ravishankara@noaa.gov.
[†] Present address: Aerodyne Research, Inc., Billerica, MA 01821.

10.1021/jp053918r CCC: $33.50
Published on Web 12/09/2005

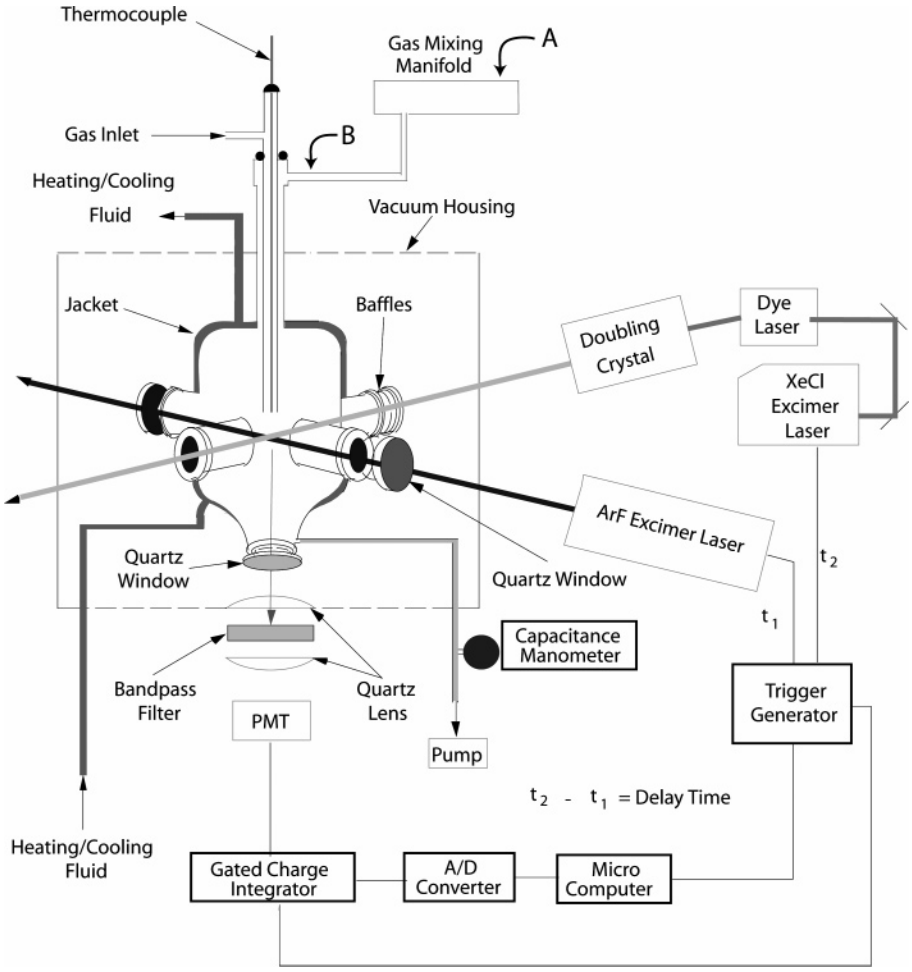

Figure 1. Schematic of the experimental apparatus used to measure k_1 and k_2. See text for details regarding the points marked A and B where NO_2 was added.

Figure 1 shows a schematic of the apparatus employed to measure k_1 and k_2. Dilute mixtures of the SH/SD precursor (RSH/RSD, where R is CH_3/CD_3 or H/D) in N_2 and/or He were flowed through the cell. Varying amounts of NO_2 were added to this mixture just upstream of the reaction cell. The flow rates of the carrier gases were measured using calibrated electronic mass flow meters. The gas mixture passed through the reaction cell with a linear flow velocity between 13 and 50 cm s^{-1}. For several experiments, O_2 was also added to this gas mixture. The total pressure in the reactor was between 30 and 120 Torr. Pressure was measured using a calibrated capacitance manometer. A heated or cooled liquid from a temperature-controlled circulator was flowed through the jacket around the reaction cell to maintain the reactor at any desired temperature. The temperature of the gas mixture in the middle of the reactor was measured using a retractable calibrated chromel−alumel thermocouple. The temperature was varied from 240 to 360 K.

Ultrahigh purity grade N_2, He, and O_2 (purities of >99.9995%, >99.9%, and >99.99%, respectively) as well as the photolytic precursors H_2S, D_2S, and CH_3SH (manufacturer's stated purities of >99% each) from Scott Specialty Gases were used without further purification. NO_2 was prepared by reacting purified NO with excess O_2, which was introduced through a molecular sieve trap maintained at dry ice temperatures. NO_2 was collected in a trap cooled to dry ice temperature. It was purified by trap-to-trap distillation in the presence of O_2 until a pure white solid remained. The major impurities in our sample of NO_2 were NO and O_2, each at a level of <0.1%. The rate coefficients[4,8] for the reactions of SH/SD with NO and O_2 are respectively $<2 \times 10^{-12}$ and 4×10^{-19} cm^3 $molecule^{-1}$ s^{-1}. At the concentrations of NO_2 used in our experiments, the NO and O_2 impurities in NO_2 were too small to make significant contributions to the measured SH/SD loss rate coefficients. The ACS spectrophotometric grade dimethyl sulfoxide (>99.9% pure), used to generate the excitation spectrum of SO, was purchased from Aldrich Chemicals and used without further purification.

Over the course of the experiments, we became suspicious that H_2S and NO_2 were reacting on the surfaces of the gas manifold because we saw a feature in the LIF spectrum that did not belong to SH. Therefore, we took a great deal of care to minimize the reaction of H_2S with NO_2 and also used CH_3SH as a source of SH in some experiments. These factors are discussed later. NO_2 concentrations were determined by absorption at 365 nm. Two different schemes were employed for the reactant and photolytic precursor; they are described later.

Photolysis of H_2S and CH_3SH at 193 nm was used to generate SH radicals. The fluence of the photolysis laser was measured using a calibrated thermopile detector. For all experiments, the initial radical concentration was estimated by using the known absorption cross section of H_2S/CH_3SH and the quantum yield for SH production, along with the measured photolysis fluence and the concentration of H_2S/CH_3SH. In all cases, the initial concentration of SH, $[SH]_0$, was less than 3×10^{12} molecules cm^{-3}, and typically 1×10^{11} cm^{-3}. The higher concentrations (10^{12} cm^{-3}) were used when SH was detected using weaker spectral features. The absorption cross sections at 193 nm of H_2S, D_2S, and CH_3SH, used to estimate $[SH]_0$ and $[SD]_0$, were 6.4×10^{-18}, 7.4×10^{-18}, and 1.86×10^{-18} cm^2, respectively.[9−13]

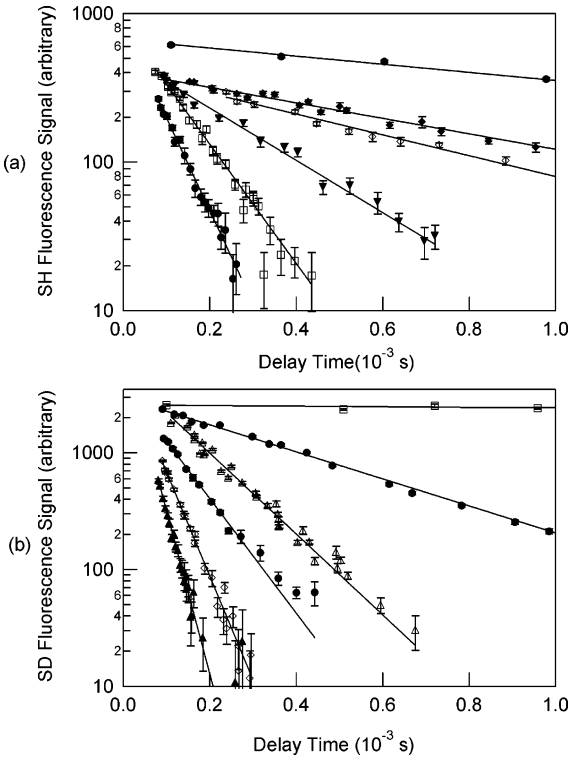

Figure 2. Temporal profiles of SH (a) and SD (b) at room temperatures. These figures show the fluorescence of SH and SD as a function of delay time.

The quantum yield of SH from the 193 nm photolysis of H_2S is assumed to be 1.[13] We measured the quantum yield for SH in CH_3SH photolysis (at 193 nm) to be 0.5 ± 0.1. This value is consistent with the quantum yield for CH_3S from CH_3SH photolysis (0.48 ± 0.05).[11]

The temporal profiles of SH and SD were monitored by pulsed laser-induced fluorescence (LIF). The output from an excimer pumped dye laser was frequency doubled to obtain wavelengths of 320 to 330 nm. The dye laser was scanned to pump the individual rotational lines of the (0,0) band of the ($A^2\Sigma$, $v' = 0$) ← ($X^2\Pi$, $v'' = 0$) transition of the SH or SD radical. The probe beam had a pulse width of ~15 ns (fwhm) and a line width of ~0.005 nm (0.1 cm^{-1}). The probe beam was passed through the reaction cell to intersect the photolysis beam; the volume created by the intersection of the two beams is referred to here as the reaction zone. The fluorescence of the thiol radical corresponding to the ($A^2\Sigma$, $v' = 0$) → ($X^2\Pi$, $v'' = 1$) transitions was collected along the third orthogonal axis using a set of lenses. The fluorescence was passed through a band-pass filter (355 ± 12 and 345 ± 10 nm for SH and SD, respectively) before it was imaged onto a photomultiplier tube (PMT). The output of the PMT was fed into a gated charge integrator. The integrated signal was sent to a personal computer via an A/D converter for signal averaging. Typically, signals from 100 laser pulses were averaged at each reaction time.

The detection sensitivities of both SH and SD were estimated using the initial signal level (temporal profile was extrapolated back to $t = 0$), the measured photolysis fluence, and the measured precursor concentration. In 100 Torr of N_2, the detection limit for SH was $<1 \times 10^9$ molecules cm^{-3}, while that for SD was $<5 \times 10^7$ molecules cm^{-3}; the better sensitivity for SD is due to the much longer fluorescence lifetime of SD ($\tau = 260$ ns[14]), which predissociates much less than SH. The $A^2\Sigma^+$ state of SH is highly predissociative with a radiative lifetime of only 3 ns[14] for $v' = 0$. This short lifetime ultimately limited its detection sensitivity. A benefit of the short lifetime was that the effect of fluorescence quenching by the bath gases (such as N_2) was essentially negligible and the detection sensitivity was nearly independent of pressure.

In kinetics measurements, the probe laser was tuned to a specific feature in the LIF spectrum and left on that feature while the delay time between the photolysis and probe lasers was varied to obtain a temporal profile. All temporal profiles of SH and SD were measured under pseudo-first-order conditions. The temporal profiles of the LIF signal followed equation I (when SH detection was not contaminated by an interfering species, as discussed later):

$$S_t = S_0 e^{-k^I t} \quad \text{(I)}$$

where S_t and S_0 are LIF signals at time t and zero and k^I is the first-order rate coefficient for the loss of SH or SD. Some typical temporal profiles of both SH that is not influenced by interferences noted later and SD are shown in Figure 2. The bimolecular rate constants, k_1 and k_2, were determined using the following analysis of the observed temporal profiles. To avoid redundancy, the determination of k_1 is detailed below, but identical procedures were used to obtain k_2. LIF signals at various reaction times were fit to eq II using a linear least-squares routine.

$$\ln(S_t) = \ln(S_0) - k^I t \quad \text{(II)}$$

This first-order rate coefficient is attributed to the sum of the following reactions that contribute to the loss of SH: reaction with NO_2, self-reaction, reaction with any impurities in the reactor, diffusion out of the reaction zone, and reaction with other species generated via laser photolysis.

$$\text{SH} + \text{NO}_2 \rightarrow \text{products} \quad (1)$$

$$\text{SH} + \text{SH} \rightarrow \text{products} \quad (3)$$

$$\text{SH} + \text{impurities} \rightarrow \text{products} \quad (4)$$

$$\text{SH} \rightarrow \text{diffusion from reaction zone} \quad (5)$$

$$\text{SH} + \text{X} \rightarrow \text{products} \quad (6)$$

X in reaction 6 is a photoproduct (e.g., $O(^3P)$ and NO) produced in the system whose concentration increases proportionately with that of NO_2. Loss of SH via processes 3−5 is represented as the first-order rate coefficient k_d. Note that reaction 3 is second order in SH; however, over the time scales of the measurements and the initial SH concentrations used in our experiments, we approximate this as a first-order process. The overall first-order SH decay rate constant is described by

$$k^I = k_d + k'_1 + k'_X = k_d + (k'_X + k_1) \times [\text{NO}_2] \quad \text{(III)}$$

The first-order loss rate coefficient k^I was measured as a function of NO_2 concentration. Typically, NO_2 was varied between 0.5×10^{13} and 20×10^{13} molecules cm^{-3}. k_d was assumed to be constant, while NO_2 was varied. The rate coefficient ($k_1 + k_X$) was derived from a linear least-squares fit of the measured values of k^I at various concentrations of NO_2 to eq III. In Figure 3, k^I is plotted against NO_2 under several experimental conditions, for both SH and SD at room temperature. The measured value of $k_1 + k_X$ was independent of photolysis fluence, and

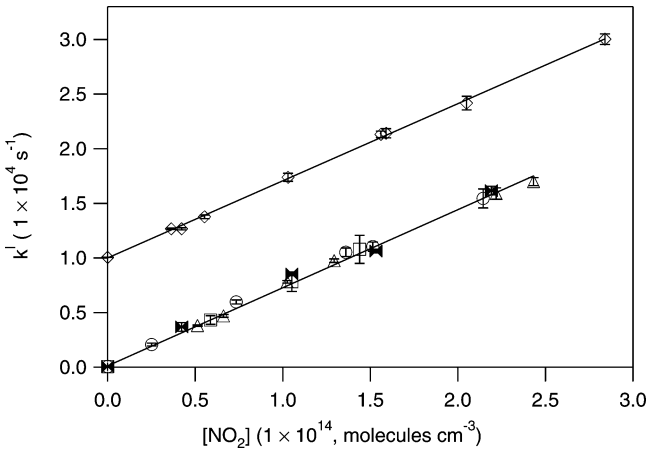

Figure 3. Plots of measured values of k^I for the removal of SH (lower line) and SD (upper line) versus NO_2 concentration at room temperature. The diamonds representing k_2 (upper line) have been offset by 10^4 s^{-1} for visual clarity. The points in the lower curve were measured under different concentrations of O_2 in the reaction cell and different photolysis fluences: (a) In 80 Torr of O_2; circles ~1 mJ $pulse^{-1}$ cm^{-2}; squares ~0.1 mJ $pulse^{-1}$ cm^{-2}; diamonds ~2 mJ $pulse^{-1}$ cm^{-2}. (b) In the absence of O_2; triangles. Each of these measurements was carried out by either properly accounting for the SO interference beneath the SH LIF transition or in the absence of such an interference, as described in the text. The figure shows that k_1 is approximately equal to k_2.

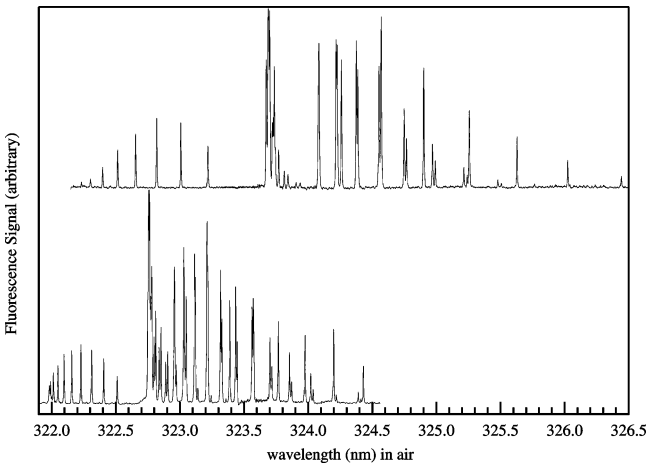

Figure 4. Excitation spectra of SH and SD. The two traces shown are the thermal excitation spectra of SH (upper trace) and SD (lower trace). The data in these spectra were taken at a delay time of 100 μs in a total pressure of 100 Torr of N_2. The photolysis of H_2S and D_2S at 193 nm generated SH and SD, respectively. The concentrations of precursor and photolysis fluence were such that [SH] ~ 3×10^{12} molecules cm^{-3} and [SD] ~ 5×10^9 molecules cm^{-3}.

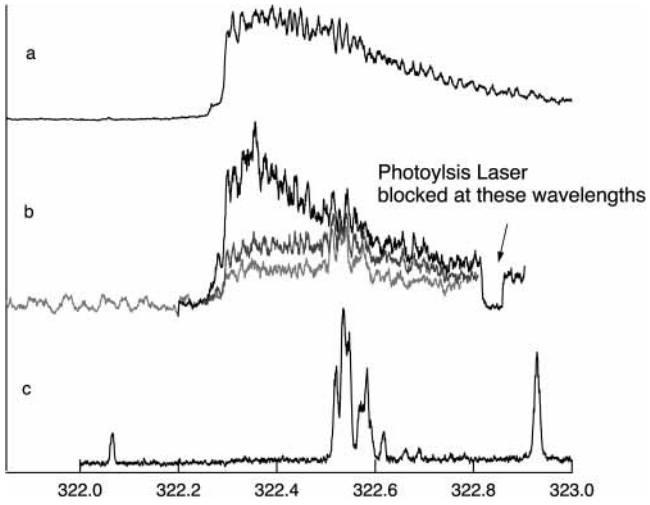

Figure 5. Spectra obtained from the photolysis of DMSO and mixtures of NO_2 and H_2S. The spectrum marked "a" shows the result of the photolysis of dimethyl sulfoxide at 193 nm without any change in the instrument settings optimized for detection of the SH radical. Trace a is the excitation spectrum of the SO radical. The spectrum "b" shows the excitation spectra when NO_2 and H_2S are photolyzed together. The spectrum "c" shows the excitation spectrum taken after cleaning the glassware involved in the instrument but prior to the introduction of NO_2 to the system.

therefore, [X] is assumed to be negligible. The measured value of the slope of the plots, as depicted in Figure 3, is therefore only k_1.

Results and Discussion

Different types of experiments were carried out during this study. The results of each type of study are described and discussed together. First, the excitation spectra of SH and SD, along with the interference in the detection of SH, is described. Second, the experimental methods used to minimize the influence of the interference in deriving kinetics data are presented. Finally, the influences of secondary reactions on the measured values of k_1 and k_2 are considered and our values of k_1 and k_2 are compared with those from previous reports.

Excitation Spectra of SH and SD. The excitation spectra of SH and SD are shown in Figure 4. Each of the six rotational branches anticipated for the ($^2\Sigma \leftarrow {}^2\Pi$) transitions are present in both spectra. The line positions are consistent with other published spectra.[10,15] The relative intensities of the rovibronic lines in this spectrum show that SH/SD is rotationally thermalized. This indicates that a delay time of 100 μs in ~100 Torr of N_2 was sufficient for rotational thermalization. The blue shift of the SD band heads is expected on the basis of the potential energy surface of the $^2\Sigma$ state. Also, as expected, the centrifugal distortion effect on the rotational line spacing is more apparent in SD than in SH.

Typically, when measuring rate constants by laser-induced fluorescence, the excitation wavelength is set to match the strongest feature in the spectrum and is not changed during the kinetics experiments. In SH, the transition that led to high detection sensitivity was the beginning of the $^RQ_{21}$ and $^QR_{21}$ branches at 323.7 nm. When H_2S and NO_2 were flowed together and photolyzed, a fluorescence feature emerged near 323.4 nm that is not due to SH. The broad feature is inconsistent with the anticipated excitation spectrum of SH, a diatomic molecule with a rotational constant greater than 8 cm^{-1}. Also, it is not present in the LIF spectrum of SH reported by Weiner et al.,[10] who generated SH in the absence of NO_2. This feature was present under some conditions used in this work as well as in the study of Black.[16] Black noted unusual behavior of the "SH signal" level when NO_2 and H_2S were mixed but did not investigate it further. We found that qualitatively the magnitude of this feature was greatly diminished when the glassware in the system was cleaned. Furthermore, this feature was visibly enhanced by the presence of NO_2. In Figure 5, the scale of the excitation spectra is expanded in wavelength to clearly show this feature. In the lowest panel, part c, a "clean" excitation spectrum obtained in the absence of NO_2 is shown. In the middle panel, part b, excitation spectra obtained in varying amounts of NO_2 are shown. The feature is clearly visible, and its magnitude increases with the NO_2 concentration ($(0.6-3.8) \times 10^{14}$ cm^{-3}). Note that, in one of the traces, the photolysis laser was temporarily blocked while the excitation wavelength continued to scan. The signal clearly returns to zero. When the photolysis laser was unblocked,

TABLE 1: Experimental Results (k_1 and k_2)

source	concn (molecules cm^{-3})	photolysis (mJ cm^{-2} $pulse^{-1}$)	[SH] (molecules cm^{-3})	LIF line	LIF wavelength[a] (nm)	$[O_2]$ (Torr)	total pressure (Torr)	NO_2 method[b]	$[NO_2]$ range (10^{13} molecules cm^{-3})	# of k'		temp (K)	$k_i \pm \sigma$ (10^{-11} cm^3 $molecule^{-1}$ s^{-1})
H_2S	9×10^{13}	0.4	2×10^{11}	R_1	323.7		83	flow	0.3−21	15	*c*	248	8.1 ± 0.4
CH_3SH	3×10^{14}	1.3	7×10^{11}	$P_{3/2}$	323.0	80	91	abs	3−22	9		252	8.1 ± 0.5
CH_3SH	5×10^{14}	0.3	3×10^{11}	R_1	323.7		85	flow	0.5−15	5		253	8.6 ± 0.7
CH_3SH	3×10^{14}	2	1×10^{12}	$P_{3/2}$	323.0	>1	92	abs	4−26	5		254	8.6 ± 0.6
CH_3SH	1×10^{14}	0.05−1.1	8×10^{10}	R_1	323.7		98	flow	0.3−28	12		263	7.6 ± 0.9
CH_3SH	2×10^{14}	0.1	4×10^{10}	R_1	323.7		99	flow	0.25−26	10		272	7.8 ± 0.7
H_2S	7×10^{13}	*	$<1 \times 10^{12}$	R_1	323.7		85	flow	2.5−25	27	*c*	295	7.0 ± 0.3
H_2S	1×10^{14}	0.3	2×10^{11}	R_1	323.7	52	70	flow	0.7−11	7	*c*	296	7.5 ± 0.6
H_2S	4×10^{13}	1.5	4×10^{11}	R_1	323.7		50	abs	0.2−12	9	*c*	296	7.1 ± 0.5
H_2S	1×10^{14}	0.3	2×10^{11}	R_1	323.7		91	flow	0.7−19	9	*c*	297	7.4 ± 0.8
H_2S[d]	8×10^{13}	0.15	8×10^{10}	R_1	323.7		100	flow	0.9−6	4	*d*	297	4.9 ± 0.5
CH_3SH	2×10^{14}	0.1	3×10^{10}	R_1	323.7		99	flow	0.5−32	12		297	7.2 ± 0.3
CH_3SH	1×10^{15}	1.2	2×10^{12}	$P_{3/2}$	323.0	>0.013	85	abs	0.4−27	13		317	6.7 ± 0.8
CH_3SH	7×10^{14}	1	1×10^{12}	$P_{3/2}$	323.0	>0.14	87	abs	3−17	8		335	6.3 ± 0.7
CH_3SH	9×10^{14}	2	3×10^{12}	$P_{3/2}$	323.0	0.5	88	abs	1−23	5		358	5.9 ± 0.7
D_2S	3×10^{13}	0.4	2×10^{10}	$R_1(D_2S)$	322.8	10	56	abs	5−35	9		246	8.4 ± 0.3
D_2S	3×10^{13}	0.5	3×10^{10}	$R_1(D_2S)$	322.8	10	57	abs	5−40	7		256	7.8 ± 0.4
D_2S	3×10^{13}	0.3	2×10^{10}	$R_1(D_2S)$	322.8	10	57	abs	6−32	10		277	7.1 ± 0.3
D_2S	8×10^{13}	0.1	1×10^{10}	$R_1(D_2S)$	322.8	>0.05	87	abs	3−19	9		297	6.3 ± 0.3
D_2S	2×10^{14}	0.08	3×10^{10}	$R_1(D_2S)$	322.8	10	60	abs	4−22	7		298	6.7 ± 0.3
D_2S	8×10^{13}	0.4	6×10^{10}	$R_1(D_2S)$	322.8	10	70	abs	4−28	5		329	6.7 ± 0.4
D_2S	7×10^{13}	0.3	4×10^{10}	$R_1(D_2S)$	322.8	10	68	abs	3−26	6		359	5.5 ± 0.4

[a] The approximate wavelength of the LIF transition is given in this column. [b] This column specifies the method used to determine $[NO_2]$. "Flow" implies the concentration was determined through a measurement of the standard mass flow rate; "abs" implies the concentration was determined through an absorption measurement. See text for additional details. [c] This measurement has accounted for the SO interference in the detection of SH by measuring the SO signal at long reaction time. See text for additional details. [d] This measurement did not account for the SO interference in detecting SH. See text for details. This measurement is not included in the calculation of our recommended value of k_1.

the "interference" returned. This sequence of experiments provides further proof that the feature is due to laser-induced fluorescence of some species generated upon photolysis either due to photodissociation of a species other than H_2S or a rapid reaction of a photolytically produced molecule. Furthermore, the prompt production of the signal strongly suggests that it is formed by the photolysis of a species produced via heterogeneous reaction between H_2S and NO_2. Note that when H_2S (SH precursor) was turned off, the feature was greatly diminished, even in the presence of NO_2. The top panel, spectrum a, shows the laser-induced fluorescence spectrum of SO ($\sim 2 \times 10^{12}$ cm^{-3}) generated through the photolysis of dimethyl sulfoxide ($(CH_3)_2SO$, DMSO) at 193 nm.[17] The concentration of SO was estimated using the known UV cross section of DMSO, the measured laser fluence, and an assumed quantum yield of unity for SO in DMSO photolysis. The similarities between the feature of SO and the interference suggests that SO is being generated and detected when H_2S and NO_2 are mixed and photolyzed.

Accuracy of the Measured Values of k_1 and k_2. When measuring temporal profiles of a reacting species, the probe laser detecting the species is typically tuned onto the signal peak and parked there when the temporal profiles are measured. In our experiments here, such a procedure would measure not only SH but also the interference "underneath" the SH signal. Therefore, to minimize the contribution of the interference to the measured value of k_1, we employed two approaches. In the first, we tuned the probe laser to one of the rotational transitions where the interference is not present. In the second, we subtracted out the contribution of the interference by detecting it at a long reaction time (five lifetimes of SH with respect to reaction 1) and assuming that the abundance of interference did not change during the course of SH reaction. The signal-to-noise ratio was lower in the first method, but no assumptions are made about the temporal behavior of the interference. The signal-to-noise ratio was larger in the second method, but it relied on the concentration of the interference species being constant. Table 1 summarizes the results of these experiments and notes the transition used. Clearly, both methods yielded essentially the same results, confirming that the contribution of the interference could be minimized. Further, the table clearly shows that the measured value of k_1 is ~20% lower when we did not account for the contribution due to the interference which we have identified to be SO and fitted the observed temporal profile to eq I.

The rate coefficients k_1 and k_2 were measured at various temperatures, and the obtained values are also listed in Table 1. Figures 6 and 7 shows our measured values of k_1 and k_2, respectively as a function of temperature, along with those from previous publications. Figure 6 also shows the lower value of k_1 at 298 K that we determined when we did not account for the SO interference. Clearly, when the interference is not accounted for, the measurement of k_1 is lower by 20%.

The SD line positions are blue shifted relative to those of SH by ~1 nm; this shift is sufficient to completely avoid detection of the SO interference. The detection sensitivity for SD was also about 2 orders of magnitude better than that for SH, and therefore, any possible contribution by the interfering species was further reduced. Thus, it was relatively straightforward to measure k_2. The measured values of k_2 are also given in Table 1. As seen in the table, within the precision of these experiments, the measured values of k_1 and k_2 are the same.

In some of the experiments, NO_2 was added to the reaction mixture prior to the main flows entering the dilution volume (added at "A" in Figure 1). In other experiments, the flow from the NO_2 bulb was diluted with N_2 and flowed through an absorption cell where the concentration of NO_2 was measured. (The absorption cross section used for NO_2 at 365 nm (in reality, two Hg lines at 365.02 and 365.48 nm) was 5.75×10^{-19} cm^2.[18]) The flow out of the absorption cell was mixed into the main flow very close to the reaction cell (added at "B" in Figure 1). This arrangement minimized the contact time between NO_2 and H_2S and, visibly, reduced the SO interference. Tests carried out using Fourier transform infrared (FTIR) spectroscopy indicated that NO_2 did react with H_2S, presumably on surfaces. A

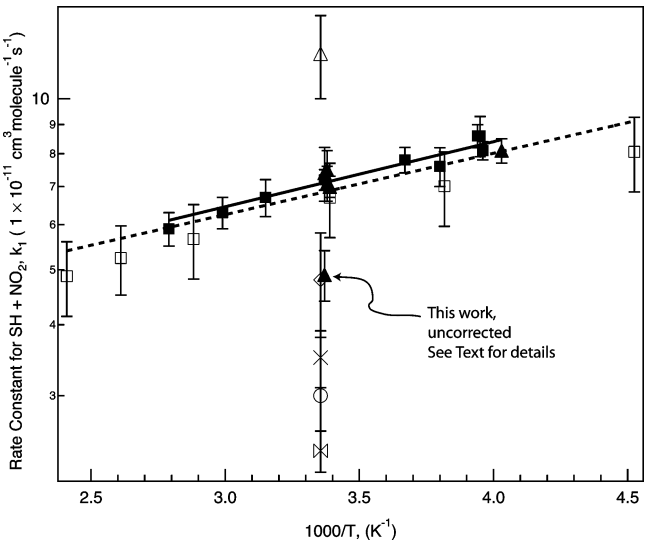

Figure 6. Arrhenius plot showing the measured values of k_1 vs 1000/*T*. The solid points are from this work; the squares were measured with CH_3SH photolysis as the SH source. The solid triangles used H_2S as the SH source. Studies of previous data from Wang et al. on k_1 are shown as open squares. The 298 K data from previous studies are the following: open triangle, Schoenle et al. (corrected by Schindler and Benter); open diamond, Stachnik and Molina; ×, Black; open circle, Friedl et al.; bow tie, Bulatov et al.

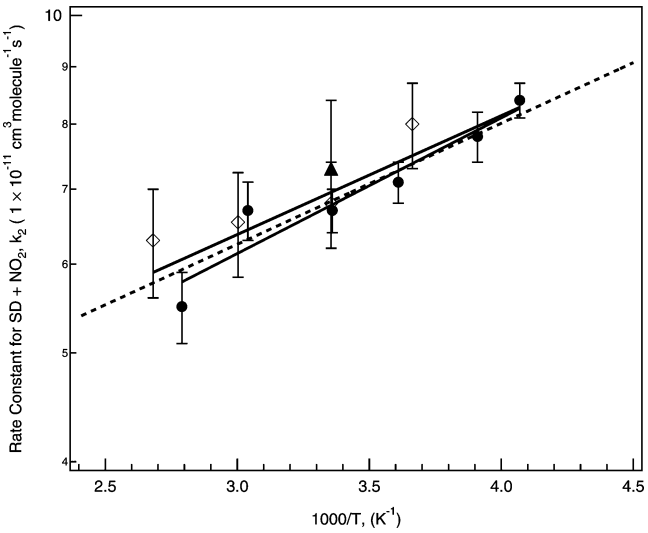

Figure 7. Arrhenius plot showing the measurements of k_2 vs 1000/*T*. The filled circles are the results of this work with D_2S photolysis as the SD source. See Table 1 for additional details regarding the filled circles in this figure. Other measurements also depicted are the following: solid triangle, Wang et al.; open diamonds, Fenter and Anderson.

sulfoxide, however, was not conclusively identified as a product of such a reaction. We did not pursue further the possible reaction of H_2S with NO_2. All of the evidence suggested that the photolysis of the product of a reaction of H_2S with NO_2 in our system was the source of the interference and that the interference was most likely SO. We could avoid the effect of the interference as discussed above when determining k_1.

Possible Influences of Secondary Reactions on the Measured Values of k_1 and k_2. When H_2S/D_2S is used as the SH/SD source, secondary reactions can potentially regenerate SH/SD on time scales of its loss due to reactions 1 and 2. The following reactions, depicted for the case of SH, are involved in determining the extent SH regeneration.

$$H_2S + h\nu(193\text{ nm}) \rightarrow H + SH \quad (7)$$

$$H_2S + H \rightarrow H_2 + SH \quad (8)$$

$$H + NO_2 \rightarrow NO + OH \quad (9)$$

$$OH + H_2S \rightarrow H_2O + SH \quad (10)$$

$$H + O_2 + M \rightarrow HO_2 + M \quad (11)$$

$$OH + NO_2 \rightarrow HNO_3 + M \quad (12)$$

In the absence of O_2, reactions 7, 9, and 10 lead to SH regeneration. Although H atoms can react with H_2S directly to form SH and H_2, this rate coefficient is rather small (8.2×10^{-13} cm^3 molecule^{-1} s^{-1} at 298 K) and, hence, H atom removal by this reaction was negligible compared to that by NO_2 and O_2 because the concentration of H_2S used in our studies was very small. In these experiments, as explained earlier, the NO_2 concentration was varied such that the lifetimes of H atoms with respect to loss due to reaction 9 varied from 33 to 2000 μs.[19] At room temperature, when 10−0.5 Torr of O_2 was present, the lifetimes of H atoms with respect to loss via O_2 association with O_2 were 10−150 μs.[19] The rate constant for reaction 10 at 298 K is $\sim 5 \times 10^{-12}$ cm^3 molecule^{-1} s^{-1} [19] which means that, at the typical concentrations of H_2S, the first-order rate constant for SH production was 500 s^{-1}. Under these conditions, with a constant [H_2S], a plot of the measured values of k^I versus NO_2 would have a negative intercept due to the regeneration of SH. Such negative intercepts were observed in the experiments where only H_2S is used as the SH source. Large concentrations of O_2 ($>3 \times 10^{17}$ cm^{-3}) suppressed regeneration because H atoms were preferentially converted to HO_2 and minimized OH production via reaction 9. Negative intercepts were not observed in the presence of large concentrations of O_2. When SH was generated via photolysis of CH_3SH, regeneration of SH was avoided. The value of k_1 measured using CH_3SH photolysis agreed with that determined using H_2S photolysis in the presence of O_2. The values of k_1 reported here were obtained by either using H_2S photolysis in the presence of O_2, accounting for the interference by subtracting the residual signal at long reaction times, or using CH_3SH photolysis as the source of SH (Table 1).

For the SD experiments, the secondary chemistry concerns are analogous to those listed above. In this work, all of the experiments were conducted in the presence of ∼10 Torr of O_2, except for one measurement at room temperature. The rate constant measured in the absence of O_2 was slightly less than that measured with O_2; however, it was essentially the same within our experimental precision. Since SO was not detected at the wavelength used for SD detection, we did not have to account for the formation of SO.

The absorption cross section of NO_2[20,21] at 193 nm is less than 5×10^{-19} cm^2. At the photolysis fluences and the concentrations of NO_2 employed in our experiments, at most, 1×10^{11} molecules cm^{-3} of O(^{1}D) and/or O(^{3}P) could be formed. At the total pressures of N_2 used in these experiments, all O(^{1}D) is expected to be quenched to O(^{3}P) within 1 μs.[19] Because the reaction of O(^{3}P) with H_2S is rather slow, the possible regeneration of SH would be at most 2 s^{-1}. The reaction of SH with O atoms could contribute at most 10 s^{-1} toward the SH loss rate constant. These effects are suppressed in the presence of NO_2, since O atoms would react with NO_2 with a pseudo-first-order loss rate constant of 200−2400 s^{-1}. The presence of ∼10 Torr of O_2 further enhances the removal of O

TABLE 2: Summary of k_1 and k_2 Determinations

method	reactor pressure (Torr)	species monitored	k_1 or k_2 at 298 K[a] (10^{-11} cm^3 molecule^{-1} s^{-1})	E_a/R (K^{-1})	reference
			k_1		
FP-LIF	30−300 He	SH	3.5 ± 0.4		Black[16]
FP-ICLA	100 Ar	HSO	2.4 ± 0.2		Bulatov et al.[25]
FP-LPA	30−730 O_2/N_2	SH	4.8 ± 1.0		Stachnik and Molina[4]
DF-LIF	2−8 He	SH	3.0 ± 0.8		Friedl et al.[24]
DF-MS	2−5 He	SH	8.6 ± 0.9		Schoenle et al.[b 23]
DF-LMR	1 He	SH	6.7 ± 1.0	-240 ± 50	Wang et al.[5]
FP-LIF	60−130 O_2/N_2	SH	7.0 ± 0.8	-270 ± 40	This Work
			k_2		
DF-LIF	2 He	SD	6.8 ± 0.6	-210 ± 70	Fenter and Anderson[22]
DF-LMR	1 He	SD	7.3 ± 1.1		Wang et al.[5]
FP-LIF	70 N_2	SD	6.6 ± 0.5	-279 ± 20	This Work

[a] The reported errors are those from the reports and may be 1σ or 2σ. Our quoted errors are at the 2σ level and included estimated systematic errors. [b] The number quoted here is the value reported by Schindler and Benter in an erratum, correcting their previously reported values in Schoenle et al. A weighted (according to their reported uncertainty in the measured first-order rate coefficient) linear least-squares analysis of the data reported by Schoenle et al. and correcting for the pressure measurement error noted in the erratum (Schindler and Benter) yields $k_1 = (7.1 \pm 0.6) \times 10^{-11}$ cm^3 molecule^{-1} s^{-1}. FP, flash photolysis; DF, discharge flow; LIF, laser-induced fluorescence; ICLA, intracavity laser absorption; LPA, long path absorption; MS, mass spectrometry; LMR, laser magnetic resonance.

atoms. Thus, the reactions of O atoms should not lead to erroneous values of k_1 or k_2. Variation of the photolysis laser fluence by a factor greater than 2 showed no change in the measured values of k_1 and k_2 (Table 1), confirming the negligible contribution of the $O(^3P) + H_2S$ reaction to SH regeneration.

Photolysis of H_2S at 193 nm can yield vibrationally excited SH radicals (up to $v'' = 12$). We estimated the quantum yield of SH($v'' = 0$) by following the temporal profile of SH($v'' = 0$) at short reaction times to be ~70% of the total SH produced in the 193 nm photolysis of H_2S; this estimate agrees with the detailed vibrational distribution of SH reported by Continetti et al.[13] We also observed that the vibrationally excited SH was quenched to the ground state by 100 Torr of N_2 with a time constant of ~15 μs. This observation leads to a phenomenological rate coefficient of $\sim 2 \times 10^{-14}$ cm^3 molecule^{-1} s^{-1} for the quenching of higher vibrational levels to the ground state. Therefore, we always employed at least 30 Torr of N_2 as the bath gas and measured the temporal profiles of SH and SD after ~60 μs while determining k_1 and k_2. The rotational distribution of photolytically produced SH was very rapidly thermalized, as shown by the invariance of the peak intensities in the excitation spectra taken at different delay times between the photolysis and probe laser. The measured values of k_1 and, by analogy, k_2 were not affected by vibrational relaxation of SH/SD during the course of SH/SD removal via reactions 1 and 2.

A summary of all of the variations in experimental parameters used in this work is shown in Table 1. They included variations in photolysis fluence and photolyte concentration, use of a different photolytic precursor, addition of O_2, and use of different spectral features for SH detection. The measured values of k_1 and k_2 did not change with the experimental precision. Therefore, we believe that our measured values of k_1 and k_2 are accurate. The average value of k_1 at 298 K measured here is $(7.24 \pm 0.62) \times 10^{-14}$ cm^3 molecule^{-1} s^{-1}, where the quoted error bars are 2σ and include an estimated uncertainty of 8% in the determination of NO_2 concentration.

Figure 6 shows our measured values of k_1 in an Arrhenius form, that is, as a plot of k_1 on a logarithmic scale versus $1/T$. These results indicate a negative temperature dependence. A fit of our data to the expression $\ln(k) = \ln(A) - E_a/(RT)$ yields the following expression:

$$k_1 = (2.87 \pm 0.50) \times 10^{-11} \exp[(270 \pm 50)/T] \text{ cm}^3 \text{ molecule}^{-1} \text{ s}^{-1}$$

In the above expression, the quoted uncertainties are 2σ. The uncertainty in A was obtained by the expression $\sigma_A = A\sigma_{\ln A}$ and by adding in quadrature an estimated systematic error of 8% due to the possible errors in the measurement of the NO_2 concentration in the reactor. A similar analysis of the data for k_2 yields

$$k_2 = (2.60 \pm 0.50) \times 10^{-11} \exp[(285 \pm 40)/T] \text{ cm}^3 \text{ molecule}^{-1} \text{ s}^{-1}$$

The measured values of k_1 and k_2 are essentially the same because the reaction involves only a secondary kinetic isotope effect. The H or D atom is essentially a spectator if the reaction proceeds via abstraction and should not influence the reaction if it is an addition process. Therefore, the measured value of k_2 is a good indicator of the value of k_1.

Discussion of This Work in Relation to Literature Values. When measuring rate constants, it is typically convenient to work under pseudo-first-order conditions. The strength of this method lies in the relative ease of measuring a purely exponential decay (or rise) of the reactant (or product) and the ability to ascribe any deviation from exponential behavior to systematic causes. The weakness is that any systematic error in the determination of the concentration of NO_2 (in this work) translates into a systematic bias in the determined k_1 value. Regarding the measurement of NO_2, there are some issues of note: the photolability of NO_2, the dimerization of NO_2 (where manometric preparation of dilute NO_2 or temperature dependent studies are concerned), and the "dark" reactivity of NO_2 itself. Due to these considerations, measuring [NO_2] itself can be difficult and may lend to the range of measured values shown in Table 2.

Depending on which type of experiment was being performed, that is, SH was generated photolytically or via discharge flow chemistry, reactions 7 and 8 act as SH sources. Reactions 8 and 10 regenerate SH, potentially hampering the determination of k_1. To suppress these regeneration sources, the addition of sufficient O_2 was employed[4] with the constraint $k_{11}[O_2][M] \gg k_9[NO_2]$. It has been proposed that O_2 could "add" to SH (similar to the addition of O_2 to CH_3S[6,7]). The effect of this adduct would be to depress the measurement of k_1. The Stachnik and Molina[4] result is ~20% less than the result of Wang et al.,[5] which is in accord with the idea that the adduct could be reducing the measured value of k_1. Work in this lab[2] has determined the

HSOO adduct to be very weak and unlikely to affect the room temperature measurement of k_1. (The upper limit for Δ^0H_{298}(association) for the formation of HSOO from HS and O_2, determined in this lab, is ~6.5 kcal mol^{-1} and will be published in a future paper.)

Only one previous study, Fenter and Anderson,[22] reported a temperature dependence of k_2. They employed a discharge flow tube to generate SD using two different sources. One was the abstraction of a deuterium atom from D_2S by a H atom, and the other was to react a deuterium atom with ethylene sulfide, which yielded SD and ethene. NO_2 was added through a movable injector at the end of the flow tube. SD was detected via laser-induced fluorescence. The results of our work are in excellent agreement with the Fenter and Anderson[22] study. The results of Wang et al.[5] on k_2 at room temperature also agree within the combined uncertainties with our value.

The history of k_1 measurements is richer than that of SD with several published studies (see Table 2). The range of measurements is great, from the product study of Bulatov et al., which reported 2.4×10^{-11} cm^3 molecule^{-1} s^{-1} to the value of 12×10^{-11} cm^3 molecule^{-1} s^{-1} found by Schoenle et al.[23] The Stachnik and Molina study suggests the measurements of Friedl et al.[24] and Black[16] suffered from the SH regeneration, as outlined earlier, and added O_2 to the reaction mixture to suppress those regeneration schemes. The Wang et al.[5] study measured k_1 as a function of temperature, using two sources of SH; the H + ethylene sulfide, already discussed, and the reaction of F with H_2S. Due to the rapidity of F + H_2S relative to the H + H_2S reaction, the regeneration of SH via reactions 8 and 10 can be minimized. It should be noted that the F atoms generated in the Wang et al. study were created through the microwave discharge of a CF_4/He mixture. Using F_2 creates difficulties, as it participates in SH regeneration via the F_2 + SH reaction. Our results agree with those of Wang et al. The source chemistry and regeneration of SH are discussed by Wang et al. and Stachnik and Molina. Therefore, the following discussion addresses only the apparent influence of SO on the measured rate coefficient.

Our discovery of an interference by SO in the detection of SH suggests that the previous studies of Stachnik and Molina and of Black may have inadvertently influenced their measured values. The results of Black et al. were influenced by secondary SH generation, as noted by others before. When the influence of the SO interference is not accounted for (see Table 1), we measured a k_1 value which is close to the result of Stachnik and Molina. It should be stated that a direct comparison of the influence of SO on the measurement of k_1 is not possible because this technique, like the work of Black and Friedl et al., is based on LIF of SH, while that of Stachnik and Molina is based on the absorption of SH. In the absorption measurement, the influence would depend on the absorption cross section of SO and SH at 323.7 nm, whereas in the LIF measurements, the relative detection sensitivity is a convolution of the absorption, fluorescence strength, and collection efficiency (mostly filler transmission). These comments regarding the influence SO has on the measurement of k_1 should not be considered as anything more than another possible difficulty associated with the measurement of k_1, by LIF at the R_1 bandhead.

Atmospheric Implications

The atmospheric lifetime of SH is determined primarily by its reaction with O_3 and NO_2. HSO is believed to be the primary product of the atmospheric oxidation of SH by both O_3 and NO_2. A SH radical in the remote clean troposphere has a lifetime of ~0.5 s (assuming 20 ppb O_3 and 0.1 ppb NO_2). This lifetime assumes that HSO, formed in the reaction of SH with O_3, will not react further with ozone to regenerate SH. In regions with higher NO_x, the lifetime of SH decreases dramatically because $k_1 \sim 20 \times k(O_3 + SH)$.

If HSO were removed mostly via its reaction with O_3 in the atmosphere, the conversion of SH to HSO followed by conversion of HSO with O_3 to give SH will form a catalytic ozone destruction cycle. However, given that only a fraction of the HSO reaction with O_3 leads to SH and that the abundances (and emissions) of H_2S to the atmosphere are rather small, we do not expect SH reaction to be a significant catalytic removal pathway for ozone. If SH is oxidized in NO_x rich regions, the formed HSO will likely be converted to HSO_2 and eventually to SO_2. Thus, in the case of either O_3 reaction or NO_2 reaction, we expect SH to be rapidly oxidized to SO_2.

Acknowledgment. This work was funded in part by NOAA's Air Quality Program.

References and Notes

(1) Berresheim, H.; Wine, P. H.; Davis, D. D. In *Composition, Chemistry and Climate of the Atmosphere*; Singh, H. B., Ed.; Van Nostrand Reinhold: New York, 1995; pp 251−307.
(2) Finlayson-Pitts, B. J.; Pitts, J. N. J. *Atmospheric Chemistry: Fundamentals and Experimental* Techniques; Wiley: New York, 1986.
(3) Seinfeld, J. H. *Atmospheric Chemistry and Physics of Air Pollution*; Wiley: New York, 1986.
(4) Stachnik, R. A.; Molina, M. J. *J. Phys. Chem.* **1987**, *91*, 4603−4606.
(5) Wang, N. S.; Lovejoy, E. R.; Howard, C. J. *J. Phys. Chem.* **1987**, *91*, 5743−5749.
(6) Laasko, D.; Smith, C. E.; Goumri, A.; Rocha, J.-D. R.; Marshall, P. *Chem. Phys. Lett.* **1994**, *227*, 377−383.
(7) Turnipseed, A. A.; Barone, S. B.; Ravishankara, A. R. *J. Phys. Chem.* **1992**, *96*, 7502−7505.
(8) Black, G.; Patrick, R.; Jusinski, L. E.; Slanger, T. G. *J. Chem. Phys.* **1984**, *80*, 4065−4070.
(9) Robert Wu, C. Y.; Chen, F. Z. *J. Quant. Spectrosc. Radiat. Transfer* **1998**, *60*, 17−23.
(10) Weiner, B. R.; Lenene, H. B.; Valentini, J. J.; Baronavski, A. P. *J. Chem. Phys.* **1989**, *90*, 1403−1413.
(11) Barone, S. B.; Turnipseed, A. A.; Gierczak, T.; Ravishankara, A. R. *J. Phys. Chem.* **1994**, *98*, 11969−11977.
(12) Butler, L. J. *Chem. Phys. Lett.* **1991**, *182*, 393−399.
(13) Continetti, R. E.; Balko, B. A.; Lee, Y. T. *Chem. Phys. Lett.* **1991**, *182*, 400−405.
(14) Friedl, R., R.; Brune Wm, H.; Anderson, J. G. *′J. Chem. Phys.* **1983**, *79*, 4227−4236.
(15) Ramsay, D. A. *J. Chem. Phys.* **1952**, *20*, 1920.
(16) Black, G. *J. Chem. Phys.* **1984**, *80*, 1103−1107.
(17) Chen, X.; Wang, H.; Weiner, B. R.; Hawley, M.; Nelson, H. H. *J. Phys. Chem.* **1993**, *97*, 12269−12274.
(18) Wine, P. H.; Kreutter, N. M.; Ravishankara, A. R. *J. Phys. Chem.* **1979**, *83*, 3191−3195.
(19) Sander, S. P.; Friedl, R. R.; Golden, D. M.; Kurylo, M. J.; Huie, R. E.; Orkin, V. L.; Moortgat, G. K.; Ravishankara, A. R.; Kolb, C. E.; Molina, M. J.; Finlayson-Pitts, B. J. *Chemical Kinetics and Photochemical Data for Use in Atmospheric Studies*, Evaluation No. 14 of NASA Panel for Data Evaluation, JPL Publication 02-25, February 2003, Pasadena CA. Available at http://jpldataeval.jpl.nasa.gov.
(20) Johnston, H. S.; Graham, R. *Can. J. Chem.* **1974**, *52*, 1415−1423.
(21) Bass, A. M.; Ledford, A. E.; Laufer, A. H. *J. Res. Natl. Bur. Stand. (U.S.)* **1976**, *80A*, 145−166.
(22) Fenter, F. F.; Anderson, J. G. *Int. J. Chem. Kinet.* **1994**, *26*, 801−812.
(23) Schoenle, G.; Rahman, M. M.; Schindler, R. N. *Ber. Bunsen-Ges. Phys. Chem.* **1987**, *91*, 66.
(24) Friedl, R. R.; Brune, W. H.; Anderson, J. G. *J. Phys. Chem.* **1985**, *89*, 5505−5510.
(25) Bulatov, V. P.; Kozliner, M. Z.; Sarkisov, O. M. *Khim. Fiz.* **1984**, *3*, 1300−1305.